IEEE Access
Multidisciplinary | Rapid Review | Open Access Journal

Received February 23, 2020, accepted March 9, 2020, date of publication March 12, 2020, date of current version March 26, 2020.

Digital Object Identifier 10.1109/ACCESS.2020.2980390

An Adaptive Super Twisting Nonlinear Fractional Order PID Sliding Mode Control of Permanent Magnet Synchronous Motor Speed Regulation System Based on Extended State Observer

PENG GAO[1,2], GUANGMING ZHANG[1], HUIMIN OUYANG[1], (Member, IEEE), AND LEI MEI[1], (Member, IEEE)

[1]College of Electrical Engineering and Control Science, Nanjing Tech University, Nanjing 211899, China
[2]College of Electrical Engineering, Tongling University, Tongling 244000, China

Corresponding author: Guangming Zhang (zgm@njtech.edu.cn)

This work was supported in part by the National Natural Science Foundation of China under Grant 61703202, and in part by the Key Research Development Project of Jiangsu Province under Grant BE2017164.

ABSTRACT In this article, a novel adaptive super-twisting nonlinear Fractional-order PID sliding mode control (ASTNLFOPIDSMC) strategy using extended state observer (ESO) for the speed operation of permanent magnet synchronous motor (PMSM) is proposed. Firstly, this paper proposes a novel nonlinear Fractional-order PID (NLFOPID) sliding surface with nonlinear proportion term, nonlinear integral term and nonlinear differential term. Secondly, the novel NLFOPID switching manifold and an adaptive super-twisting reaching law (ASTRL) are applied to obtain excellent control performance in the sliding mode phase and the reaching phase, respectively. The novel ASTNLFOPIDSMC strategy is constructed by the ASTRL and the NLFOPID sliding surface. Due to the utilization of NLFOPID switching manifold, the characteristics of fast convergence, good robustness and small steady state error can be ensured in the sliding mode phase. Due to the utilization of ASTRL, the chattering phenomenon can be weakened, and the characteristics of high accuracy and strong robustness can be obtained in the reaching phase. Further, an ESO is designed to achieve dynamic feedback compensation for external disturbance. Furthermore, Lyapunov stability theorem and Fractional calculus are used to prove the stability of the system. Finally, comparison results under different controllers demonstrate that the proposed control strategy not only achieves good stability and dynamic properties, but also is robust to external disturbance.

INDEX TERMS Adaptive super-twisting nonlinear Fractional-order PID sliding mode control (ASTNLFOPIDSMC) strategy, extended state observer (ESO), permanent magnet synchronous motor (PMSM), nonlinear Fractional-order PID (NLFOPID) sliding surface, adaptive super-twisting reaching law (ASTRL).

I. INTRODUCTION

Permanent magnet synchronous motor (PMSM) is widely used in industry applications [1]–[3]. The traditional linear controllers are widely used in the control of PMSM because of their simple structure, but due to the unknown disturbance, time-varying, strong coupling of PMSM, the traditional linear controllers cannot meet the high performance control requirements [4], [5]. Therefore, many different advanced control strategies have been proposed to improve the control performance of PMSM, such as backstepping control [6], [7], finite time control [8], model predictive control [9], fuzzy logic control [10], sliding mode control (SMC) [11]–[13] and robust control [14]. Among them, SMC has been widely used for decades, because of its robustness and simplicity. Several SMC strategies were proposed by many scholars, such as event-triggered SMC [15], adaptive SMC [16], [17], fuzzy SMC [18], [19], model free SMC [20], global SMC [21], [22], complementary SMC [23], [24], *et al.* The performance of SMC strategy mainly depends on the sliding

The associate editor coordinating the review of this manuscript and approving it for publication was Jun Shen.

mode surface and reaching law. The PID controller is a classical feedback controller. Because the PID controller has the advantages of simple structure and well-known parameter adjustment rules, the PID sliding surface has been designed by scholars to improve the control performance of the closed-loop system. The PID sliding surface is defined as the present, past and future functional forms of error signals. The SMC strategies based on different forms of PID sliding surface have been widely used in many practical systems. In [25]–[28], SMC strategies based on the PID sliding surface were developed to the process control systems, robotic manipulators, quadcopter and semi-active vehicle suspension, respectively. For 300 years, Fractional-order theory has been studied by scholars as pure mathematics theory. In recent years, the combination of Fractional-order theory and various control theories has been widely used in many systems. In [29]–[31], nonsingular terminal SMC strategies combined with the Fractional-order theory were designed for cable-driven manipulators. Fuzzy sliding mode theory combined with Fractional-order theory was proposed for uncertain Fractional-order nonlinear systems in [32]. In [33], [34], dynamic surface control strategies combined with the Fractional-order theory were designed for Fractional-order nonlinear systems. By combining the traditional PID sliding surface with the Fractional-order theory, the linear Fractional-order PID (LFOPID) sliding surface can be obtained. Compared with Integer-order, the extra degrees of freedom from using of Fractional-order integrator and differentiator made it possible to further improve the control effect [35]. Recently, many SMC strategies based on different forms of LFOPID sliding surface have been widely used in many systems, such as wind power generation system [36], wheeled mobile robot [37], electro-hydraulic servo system [38] and PMSM [39], *et al.* However the linear superposition of three basic modules in the LFOPID can cause the contradiction between the rapidity and the overshoot, and the LFOPID also has the disadvantages of simplicity and tough, which makes it difficult to meet the control requirements of high quality [40], [41]. A nonlinear function $fal(\cdot)$ was proposed by Han in [42]. It has the characteristics of fast convergence, reduce steady state error and saturated error [43]- [45]. In order to effectively settled above-mentioned issues of the LFOPID sliding surface, the nonlinear function $fal(\cdot)$ is first introduced into the conventional LFOPID sliding surface. Based on the LFOPID sliding surface and the nonlinear function $fal(\cdot)$, a novel nonlinear FOPID (NLFOPID) sliding surface is proposed with nonlinear proportion term, nonlinear integral term and nonlinear differential term in this study.

The main disadvantage of the conventional SMC is chattering phenomenon. The super-twisting (ST) scheme is one of the high-order SMC which has been made to solve the chattering problem, good control performance can be ensured by the ST scheme simultaneously [46]. However, the ST scheme requires upper bound information of the lumped uncertainties to calculate the control parameters, which is very difficult in reality. [47] proposed an adaptive super-twisting (AST) scheme. The AST scheme has advantages of addressing the unknown upper bound of the disturbance and the adaptability of control parameters. Because of the superiorities, AST scheme has been widely used in many practical systems, such as air vehicle [48], marine vessels [49], vehicle steer-by-wire system [50], cable-driven manipulators [51], rigid robotic manipulators [52], *et al.*

Since extended state observer (ESO) can effectively estimate the total disturbance of the system and rarely rely on the mathematical model of the system, it has been widely used to estimate the external disturbance in various practical systems, such as linear induction motor [45], test rocket control system [53], spacecraft [43], *et al.*

In this study, a novel adaptive super-twisting nonlinear Fractional-order PID sliding mode control (ASTNLFOPIDSMC) strategy using the ESO for the speed operation of PMSM is proposed. In order to solve the contradiction between the rapidity and the overshoot of the LFOPID sliding surface, and to solve the disadvantages of simplicity and tough of the LFOPID sliding surface, a novel NLFOPID sliding surface combining the nonlinear function $fal(\cdot)$ is proposed. Due to the utilization of the NLFOPID switching manifold, the characteristics of fast convergence, good robustness and small steady state error can be ensured in the sliding mode phase. An AST scheme is designed to suppress the chattering phenomenon of the conventional SMC and improve the control performance of the system in the reaching phase. Then, in order to improve the ability of the system to resist external disturbance, the novel ASTNLFOPIDSMC strategy utilizes the ESO to achieve dynamic feedback compensation for external disturbance.

The main contributions of this paper can be listed as follows:

1. The nonlinear function $fal(\cdot)$ is first introduced into the conventional LFOPID sliding surface. We propose a novel NLFOPID sliding surface, which includes nonlinear proportional term, nonlinear integral term and nonlinear differential term.
2. An AST scheme is selected to improve the control performance of the reaching phase. A novel ASTNLFOPIDSMC strategy is constructed by the AST scheme and the novel NLFOPID sliding surface.
3. A novel ESO based the ASTNLFOPIDSMC strategy is proposed. The ESO is designed to achieve dynamic feedback compensation for external disturbance. The proposed control strategy not only achieves good stability and dynamic properties, but also is robust to external disturbance.
4. Lyapunov stability theorem and Fractional calculus are used to prove the stability of the system.
5. The effectiveness and superiority of our proposed control scheme, compared to the existing theory, have been verified by simulation results.

The rest of this paper is organized as follows: some definitions and properties of Fractional-order calculus are presented in Section II. In Section III, the control strategies and

the stability analysis are given. The comparative results and the analysis of results are given in Section IV. Section V gives main conclusions and future work.

II. MATHEMATICAL PRELIMINARIES

This section presents some definitions and properties of Fractional-order calculus.

The Riemann-Liouville Fractional derivative and integral of function $f(t)$ are given by [54], [55]:

$$\begin{cases} {}_{t_0}D_t^{\varepsilon} f(t) = \dfrac{1}{\Gamma(1-\varepsilon)} \dfrac{d}{dt} \displaystyle\int_{t_0}^{t} \dfrac{f(\tau)}{(t-\tau)^{\varepsilon}} d\tau \\ {}_{t_0}D_t^{-u} f(t) = \dfrac{1}{\Gamma(u)} \displaystyle\int_{t_0}^{t} \dfrac{f(\tau)}{(t-\tau)^{1-u}} d\tau \\ \Gamma(z) = \displaystyle\int_0^{\infty} e^{-t} t^{z-1} dt \end{cases} \tag{1}$$

where $z \in R$; t and t_0 represent the upper and lower bounds of the Fractional derivative and integral; ε and u are the Fractional derivative order and integral order, respectively; $0 < \varepsilon, u < 1$.

The Caputo Fractional derivative of order a of function $f(t)$ is defined as follows [54], [55]:

$${}_{t_0}D_t^{a} f(t) = \begin{cases} \dfrac{1}{\Gamma(m-a)} \displaystyle\int_{t_0}^{t} \dfrac{f^{(m)}(\tau)}{(t-\tau)^{a-m+1}} d\tau & m-1 < a < m \\ \dfrac{d^m}{dt^m} f(t) & a = m \end{cases} \tag{2}$$

where m is the first integer larger than a.

Riemann-Liouville Fractional-order definition is selected in this article.

The Fractional order derivative and integral have the following properties [54], [55]:

$$\frac{d^n}{dt^n} \left({}_{t_0}D_t^{\varepsilon} f(t) \right) = {}_{t_0}D_t^{\varepsilon+n} f(t) \tag{3}$$

$$\frac{d^n}{dt^n} \left({}_{t_0}D_t^{-u} f(t) \right) = {}_{t_0}D_t^{n-u} f(t) \tag{4}$$

The Fractional order derivative has the property of linear operation [54], [55]:

$${}_{t_0}D_t^{\varepsilon} \left(af(t) + bf(t) \right) = a\, {}_{t_0}D_t^{\varepsilon} f(t) + b\, {}_{t_0}D_t^{\varepsilon} f(t) \tag{5}$$

The following autonomous system [56]:

$${}_{t_0}D_t^{\varepsilon} f(t) = Zf(t) \quad f(0) = f_0 \tag{6}$$

where $f(t) \in R^n$, $Z \in R^{n \times n}$, $0 < \varepsilon < 1$, (6) is asymptotically stable if and only if:

$$|\arg(eig(Z))| > \varepsilon \frac{\pi}{2} \tag{7}$$

Then, the components of the state decay towards 0 like $t^{-\varepsilon}$.

III. CONTROL STRATEGIES DESIGN

A. CONTROLLERS DESIGN

Equation of electromagnetic torque for PMSM can be described as follows:

$$T_e = p_n(\varphi_f i_q + (L_d - L_q) i_q i_d) \tag{8}$$

where T_e is the electromagnetic torque; φ_f is the flux linkage; p_n is the number of pole pairs; L_d, L_q represent the $d-$ and $q-$ axis inductances, respectively; i_d, i_q are the components of armature currents of $dq-$ axes, respectively.

For surface mount PMSM, $L_d = L_q = L$ in this paper, equation of mechanical torque for PMSM can be expressed as in (9), the dynamics of PMSM can be expressed as in (10). The motor tracking speed error is defined as in (11).

$$\begin{cases} T_e - T_L = \dfrac{J}{p_n} \dot{\omega} + B\omega \\ T_e = p_n \varphi_f i_q \end{cases} \tag{9}$$

$$\dot{\omega} = \frac{3 p_n \varphi_f}{2J} i_q - \frac{B}{J} \omega - \frac{1}{J} T_L \tag{10}$$

$$e = \omega_r - \omega \tag{11}$$

where e is the tracking error; ω is the mechanical rotor angular speed of PMSM; J is the rotational inertia; T_L is the load torque; B is the viscous friction coefficient; ω_r is the desired speed.

The conventional LFOPID sliding surface was defined as [38], [39]:

$$s = K_p e + K_i D_t^{-u} e + K_d D_t^{\varepsilon} e \tag{12}$$

where $K_p > 0$, $K_i > 0$, $K_d > 0$.

The structure diagram of the conventional LFOPID sliding surface (12) is shown in Fig. 1.

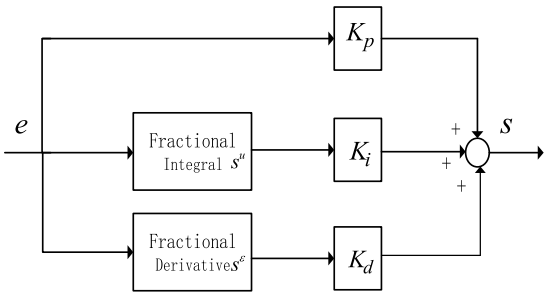

FIGURE 1. Structure diagram of traditional LFOPID sliding surface.

The following exponential reaching law (ERL) was usually chosen [38], [39]:

$$\dot{s} = -ks - \eta sign(s) \tag{13}$$

$$sign(s) = \begin{cases} 1 & s > 0 \\ 0 & s = 0 \\ -1 & s < 0 \end{cases} \tag{14}$$

where $k \in R^+$, $\eta \in R^+$.

According to (3), (4), (12) and (13), we can obtain:

$$K_p \dot{e} + K_i D_t^{1-u} e + K_d D_t^{\varepsilon+1} e = -ks - \eta sign(s) \tag{15}$$

Sequentially, substituting (10) into (15), then the following formula can be derived.

$$K_p(\dot{\omega}_r - \frac{3p_n\varphi_f}{2J}i_q + \frac{T_L}{J} + \frac{B}{J}\omega) + K_iD_t^{1-u}e + K_dD_t^{1+\varepsilon}e = -ks - \eta sign(s) \quad (16)$$

Afterwards, the conventional control law of SMC based on the conventional LFOPID sliding surface (12) and the ERL (13) (LFOPIDSMC) can be given as follows:

$$i_q = \frac{2J}{3p_n\varphi_f K_p}((K_p(\dot{\omega}_r + \frac{T_L}{J} + \frac{B}{J}\omega) + K_iD_t^{1-u}e + K_dD_t^{1+\varepsilon}e + ks + \eta sign(s)) \quad (17)$$

The proposed NLFOPID sliding surface can be defined as:

$$s = K_p fal(e,\alpha,\delta) + K_iD_t^{-u}(fal(e,\alpha,\delta)) + K_dD_t^{\varepsilon}(fal(e,\alpha,\delta)) \quad (18)$$

where $K_p > 0$, $K_i > 0$, $K_d > 0$ and $u = \varepsilon$.

The nonlinear function $fal(x,\alpha,\delta)$ was proposed by Han [42], the nonlinear function defined as:

$$fal(x,\alpha,\delta) = \begin{cases} |x|^{\alpha}sign(x) & if \ |x| > \delta \\ \dfrac{x}{\delta^{1-\alpha}} & if \ |x| \le \delta \end{cases} \quad (19)$$

where $0 < \delta < 1$ and $0 < \alpha < 1$.

The nonlinear function $fal(x,\alpha,\delta)$ has the following characteristics: when $0 < \alpha < 1$, the nonlinearity degree of $fal(x,\alpha,\delta)$ is influenced by the value of α, which can also help to reduce steady state error significantly; $fal(x,\alpha,\delta)$ shows that a larger error corresponds to a lower gain ($|fal(x,\alpha,\delta)| < |x|$), so the function has the characteristic of saturated error; $fal(x,\alpha,\delta)$ also shows that a small error corresponds to a higher gain ($|fal(x,\alpha,\delta)| > |x|$), so the nonlinear function $fal(x,\alpha,\delta)$ has the characteristic of fast convergence. Fig. 2 shows the corresponding function curves of the nonlinear function $fal(x,\alpha,\delta)$.

Based on the above information, a novel NLFOPID sliding surface is designed as below. Firstly, $fal(e,\alpha,\delta)$ is obtained by error signal e passes through the nonlinear function $fal(x,\alpha,\delta)$; then, the error signal e in the proportional term, integral term and differential term of the conventional LFOPID sliding surface is replaced by the nonlinear function $fal(x,\alpha,\delta)$ in which the contradiction between the rapidity and the overshoot by linear superposition of three basic modules in the conventional LFOPID can be overcome, the shortcomings of relatively simple and rough signal processing on the traditional LFOPID sliding surface are also compensated by the nonlinear function $fal(e,\alpha,\delta)$. Fig. 3 shows the novel NLFOPID sliding surface structure diagram.

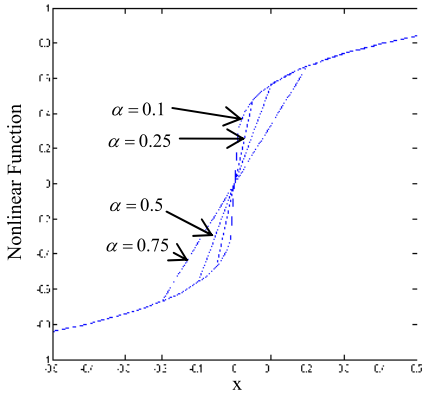

FIGURE 2. Characteristic curves of $fal(x,\alpha,\delta)$, $\delta = 0.1$, $\alpha = 0.1, 0.25, 0.5,$ and 0.75.

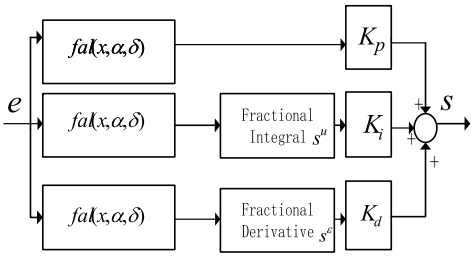

FIGURE 3. Structure diagram of the proposed NLFOPID sliding surface.

Sequentially, substituting (13) into (18), then the following can be derived.

$$\begin{cases} K_p(\alpha\,|e|^{\alpha-1}\,\dot{e}) + K_iD_t^{1-u}(fal((e,\alpha,\delta))) \\ +K_dD_t^{\varepsilon+1}(fal((e,\alpha,\delta)) \\ = -ks - \eta sign(s) & if \ |e| > \delta \\ K_p((1/\delta^{1-\alpha})\dot{e}) + K_iD_t^{1-u}(fal((e,\alpha,\delta)) \\ +K_dD_t^{\varepsilon+1}(fal((e,\alpha,\delta)) \\ = -ks - \eta sign(s) & if \ |e| \le \delta \end{cases} \quad (20)$$

The proposed SMC strategy based on the novel NLFOPID sliding surface (18) and the ERL (13) (NLFOPIDSMC) can be given as:

$$\begin{cases} K_p(\alpha\,|e|^{\alpha-1}\,(\dot{\omega}_r - \frac{3p_n\varphi_f}{2J}i_q + \frac{T_L}{J} + \frac{B}{J}\omega)) \\ +K_iD_t^{1-u}(fal((e,\alpha,\delta))) \\ \quad +K_dD_t^{\varepsilon+1}(fal((e,\alpha,\delta)) = -ks - \eta sign(s) & if \ |e| > \delta \\ K_p((1/\delta^{1-\alpha})(\dot{\omega}_r - \frac{3p_n\varphi_f}{2J}i_q + \frac{T_L}{J} + \frac{B}{J}\omega)) \\ \quad +K_iD_t^{1-u}(fal((e,\alpha,\delta)) \\ +K_dD_t^{\varepsilon+1}(fal((e,\alpha,\delta)) = -ks - \eta sign(s) & if \ |e| \le \delta \end{cases} \quad (21)$$

$$\begin{cases} i_q = \dfrac{2J}{3p_n\varphi_f K_p\alpha\,|e|^{\alpha-1}} \\ ((K_p\alpha\,|e|^{\alpha-1}\,(\dot{\omega}_r + \frac{T_L}{J} + \frac{B}{J}\omega) \\ +K_iD_t^{1-u}(fal(e,\alpha,\delta)) + K_dD_t^{1+\varepsilon}(fal(e,\alpha,\delta)) \\ +ks + \eta sign(s)) & if \ |e| > \delta \\ i_q = \dfrac{2J}{3p_n\varphi_f K_p(1/\delta^{1-\alpha})} \\ \quad ((K_p(1/\delta^{1-\alpha})(\dot{\omega}_r + \frac{T_L}{J} + \frac{B}{J}\omega) \\ +K_iD_t^{1-u}(fal(e,\alpha,\delta)) + K_dD_t^{1+\varepsilon}(fal(e,\alpha,\delta)) \\ +ks + \eta sign(s)) & if \ |e| \le \delta \end{cases} \quad (22)$$

In order to effectively suppress the chattering problem and improve the control performance in the reaching phase, the following adaptive super-twisting reaching law (ASTRL) is selected.

$$\begin{cases} \dot{s} = -\eta_1 |s|^{1/2} sign(s) + \eta_2 \\ \dot{\eta}_2 = -\dfrac{\beta}{2} sign(s) \end{cases} \tag{23}$$

where the adaptive control term is constructed as:

$$\begin{cases} \dot{\eta}_1 = \begin{cases} \gamma_1 \sqrt{\dfrac{\kappa_1}{2}} sign(|s| - \nu) & if\ \eta_1 > \hat{\eta}_1 \\ \Re & if\ \eta_1 \le \hat{\eta}_1 \end{cases} \\ \beta = 2\theta\eta_1 \end{cases} \tag{24}$$

where γ_1, κ_1, ν, θ, $\Re$ and $\hat{\eta}_1$ are the positive coefficients.

Remark 1: $\hat{\eta}_1$ and $\Re$ are arbitrary small positive coefficients, large γ_1, κ_1, θ and small ν can obtain smaller tracking error and larger convergence rate.

According to (18) and (23), we can obtain:

$$\begin{cases} K_p(\alpha |e|^{\alpha-1} \dot{e}) + K_i D_t^{1-u}(fal((e, \alpha, \delta))) \\ \quad + K_d D_t^{\varepsilon+1}(fal((e, \alpha, \delta)) \\ = -\eta_1 |s|^{1/2} sign(s) + \eta_2 \qquad if\ |e| > \delta \\ K_p((1/\delta^{1-\alpha})\dot{e}) + K_i D_t^{1-u}(fal((e, \alpha, \delta)) \\ \quad + K_d D_t^{\varepsilon+1}(fal((e, \alpha, \delta)) \\ = -\eta_1 |s|^{1/2} sign(s) + \eta_2 \qquad if\ |e| \le \delta \end{cases} \tag{25}$$

Afterwards, the proposed SMC strategy based on the novel NLFOPID sliding surface (18) and the ASTRL (23), (24) (ASTNLFOPIDSMC) can be given as follows:

$$\begin{cases} K_p(\alpha |e|^{\alpha-1} (\dot{\omega}_r - \dfrac{3p_n\varphi_f}{2J} i_q + \dfrac{T_L}{J} + \dfrac{B}{J}\omega)) \\ \quad + K_i D_t^{1-u}(fal((e, \alpha, \delta))) \\ + K_d D_t^{\varepsilon+1}(fal((e, \alpha, \delta)) \\ \quad = -\eta_1 |s|^{1/2} sign(s) + \eta_2 \qquad if\ |e| > \delta \\ K_p((1/\delta^{1-\alpha})(\dot{\omega}_r - \dfrac{3p_n\varphi_f}{2J} i_q + \dfrac{T_L}{J} + \dfrac{B}{J}\omega)) \\ \quad + K_i D_t^{1-u}(fal((e, \alpha, \delta)) \\ + K_d D_t^{\varepsilon+1}(fal((e, \alpha, \delta)) \\ \quad = -\eta_1 |s|^{1/2} sign(s) + \eta_2 \qquad if\ |e| \le \delta \end{cases} \tag{26}$$

$$\begin{cases} i_q = \dfrac{2J}{3p_n\varphi_f K_p \alpha |e|^{\alpha-1}} \\ \quad ((K_p\alpha |e|^{\alpha-1} (\dot{\omega}_r + \dfrac{T_L}{J} + \dfrac{B}{J}\omega) \\ + K_i D_t^{1-u}(fal(e, \alpha, \delta)) + K_d D_t^{1+\varepsilon}(fal(e, \alpha, \delta)) \\ + \eta_1 |s|^{1/2} sign(s) - \eta_2) \qquad if\ |e| > \delta \\ i_q = \dfrac{2J}{3p_n\varphi_f K_p(1/\delta^{1-\alpha})} \\ \quad ((K_p(1/\delta^{1-\alpha})(\dot{\omega}_r + \dfrac{T_L}{J} + \dfrac{B}{J}\omega) \\ + K_i D_t^{1-u}(fal(e, \alpha, \delta)) + K_d D_t^{1+\varepsilon}(fal(e, \alpha, \delta)) \\ + \eta_1 |s|^{1/2} sign(s) - \eta_2) \qquad if\ |e| \le \delta \end{cases} \tag{27}$$

where load torque T_L is estimated by an ESO in this paper.

According to Equation (10), define $x_1 = \omega$ and $x_2 = -T_L/J$, Equation (10) can be rewritten as:

$$\begin{cases} \dot{x}_1 = x_2 - \dfrac{B}{J} x_1 + \dfrac{3p_n\varphi_f}{2J} i_q \\ \dot{x}_2 = \vartheta \end{cases} \tag{28}$$

where ϑ can be regarded as disturbance of x_2.

The ESO is designed as follows:

$$\begin{cases} \bar{e} = Z_{21} - x_1 \\ \dot{Z}_{21} = Z_{22} - \tilde{\beta}_{01} fal(\bar{e}, \delta, \alpha) + \tilde{b}_0 i_q \\ \dot{Z}_{22} = -\tilde{\beta}_{02} fal(\bar{e}, \delta, \alpha) \end{cases} \tag{29}$$

where $\tilde{\beta}_{01}$ and $\tilde{\beta}_{02}$ are the positive gain parameters of the ESO; $\tilde{b}_0$ is an estimation of the compensation factor; Z_{21} and Z_{22} are used to estimate the values of x_1 and x_2, respectively; the unknown disturbance $-T_L/J = Z_{22} - \Delta d$, and Δd is the estimation error.

Remark 2: In general, the gain parameters of the ESO are selected as $\tilde{\beta}_{01} = 2\omega_0$, $\tilde{\beta}_{02} = \omega_0^2$,which can achieve a good prediction effect, where ω_0 is the bandwidth of the ESO.

According to (29), (22) could then be expressed by the following:

$$\begin{cases} i_q = \dfrac{2J}{3p_n\varphi_f K_p \alpha |e|^{\alpha-1}} \\ \quad ((K_p\alpha |e|^{\alpha-1} (\dot{\omega}_r - Z_{22} + \dfrac{B}{J}\omega) \\ + K_i D_t^{1-u}(fal(e, \alpha, \delta)) + K_d D_t^{1+\varepsilon}(fal(e, \alpha, \delta)) \\ + ks + \eta sign(s)) \qquad if\ |e| > \delta \\ i_q = \dfrac{2J}{3p_n\varphi_f K_p(1/\delta^{1-\alpha})} \\ \quad ((K_p(1/\delta^{1-\alpha})(\dot{\omega}_r - Z_{22} + \dfrac{B}{J}\omega) \\ + K_i D_t^{1-u}(fal(e, \alpha, \delta)) + K_d D_t^{1+\varepsilon}(fal(e, \alpha, \delta)) \\ + ks + \eta sign(s)) \qquad if\ |e| \le \delta \end{cases} \tag{30}$$

According to (29), (27) could then be expressed by the following:

$$\begin{cases} i_q = \dfrac{2J}{3p_n\varphi_f K_p \alpha |e|^{\alpha-1}} \\ \quad ((K_p\alpha |e|^{\alpha-1} (\dot{\omega}_r - Z_{22} + \dfrac{B}{J}\omega) \\ + K_i D_t^{1-u}(fal(e, \alpha, \delta)) + K_d D_t^{1+\varepsilon}(fal(e, \alpha, \delta)) \\ + \eta_1 |s|^{1/2} sign(s) - \eta_2) \qquad if\ |e| > \delta \\ i_q = \dfrac{2J}{3p_n\varphi_f K_p(1/\delta^{1-\alpha})} \\ \quad ((K_p(1/\delta^{1-\alpha})(\dot{\omega}_r - Z_{22} + \dfrac{B}{J}\omega) \\ + K_i D_t^{1-u}(fal(e, \alpha, \delta)) + K_d D_t^{1+\varepsilon}(fal(e, \alpha, \delta)) \\ + \eta_1 |s|^{1/2} sign(s) - \eta_2) \qquad if\ |e| \le \delta \end{cases} \tag{31}$$

Compared with the traditional LFOPIDSMC (17), the ASTNLFOPIDSMC (31) proposed in this paper has

the following advantages: 1) the disadvantages by linear superposition of three basic modules in the conventional LFOPID sliding surface can be overcome by the nonlinear function $fal(e, \alpha, \delta)$ in the sliding mode phase; 2) the ASTRL can effectively solve the chattering problem of the traditional LFOPIDSMC, good control performance can be ensured by the ASTRL in the reaching phase simultaneously; 3) load torque estimated by the ESO transferred to the drive system, which can improve the ability of the system to resist external disturbance.

In this study, a novel compound control strategy is designed for the PMSM speed regulation system with $i_d = 0$ control strategy is shown in Fig. 4. The block diagrams of the NLFOPIDSMC and ASTNLFOPIDSMC schemes are shown in Fig. 4 (b), Fig. 4 (c), respectively.

B. STABILITY ANALYSIS

The stability of the proposed NLFOPIDSMC is discussed in the following theorem.

Proof: Step 1: the positive definite Lyapunov function can be constructed as:

$$V = \frac{1}{2}s^2 > 0 \tag{32}$$

Taking the first derivative of (32), we have:

$$\begin{aligned}\dot{V} &= s \cdot \dot{s} \\ &= s(K_p D_t^1 fal(e, \alpha, \delta) + K_i D_t^{1-u} fal(e, \alpha, \delta) \\ &\quad + K_d D_t^{\varepsilon+1} fal(e, \alpha, \delta))\end{aligned} \tag{33}$$

According to (19), (33) could be expressed by the following:

Then, substituting (30) into (34), as shown at the bottom of this page, it can be obtained as:

$$\begin{aligned}\dot{V} &= \begin{cases} s\left(-ks - \eta sign(s) + K_p\alpha\,|e|^{\alpha-1}\,\Delta d\right) & if\ |e| > \delta \\ s\left(-ks - \eta sign(s) + K_p(1/\delta^{1-\alpha})\Delta d\right) & if\ |e| \le \delta \end{cases} \\ &= \begin{cases} -ks^2 - sign(s)\eta s + K_p\alpha\,|e|^{\alpha-1}\,s\Delta d & if\ |e| > \delta \\ -ks^2 - sign(s)\eta s + K_p(1/\delta^{1-\alpha})s\Delta d & if\ |e| \le \delta \end{cases} \\ &= \begin{cases} -ks^2 - \eta\,|s| + K_p\alpha\,|e|^{\alpha-1}\,s\Delta d & if\ |e| > \delta \\ -ks^2 - \eta\,|s| + K_p(1/\delta^{1-\alpha})s\Delta d & if\ |e| \le \delta \end{cases}\end{aligned} \tag{35}$$

Assumption 1: In practice, the disturbances are bounded, so we can get the following bounded conditions:

$$\begin{cases} \Delta d \le \Xi \\ K_p\alpha\,|e|^{\alpha-1}\,\Xi < \eta \\ K_p(1/\delta^{1-\alpha})\Xi < \eta \end{cases} \tag{36}$$

where Ξ is the upper limit of Δd, and it is a constant.

According to Assumption 1, one can rewrite (35) in the following form:

$$\dot{V} \le \begin{cases} -ks^2 - \eta\,|s| + |s|\,K_p\alpha\,|e|^{\alpha-1}\,\Xi < 0 & if\ |e| > \delta \\ -ks^2 - \eta\,|s| + |s|\,K_p(1/\delta^{1-\alpha})\Xi < 0 & if\ |e| \le \delta \end{cases} \tag{37}$$

Thus, it has been proved that with the proposed NLFOPIDSMC law, the system can reach the sliding surface at any initial state.

Step 2: When the system reaches the sliding surface, the following formula is satisfied.

$$\begin{aligned}&K_p(fal(e, \alpha, \delta)) + K_i D_t^{-u}(fal(e, \alpha, \delta)) \\ &\qquad + K_d D_t^{\varepsilon}(fal(e, \alpha, \delta)) = 0\end{aligned} \tag{38}$$

According to (5), Equation (38) can be taken by the Fractional derivative of order ε written as follows:

$$\begin{aligned}&K_p D_t^{\varepsilon}(fal(e, \alpha, \delta)) + K_i(fal(e, \alpha, \delta)) \\ &\qquad + K_d D_t^{\varepsilon}(D_t^{\varepsilon}(fal(e, \alpha, \delta))) = 0\end{aligned} \tag{39}$$

The sliding mode dynamics also can be obtained by the Equation (40).

$$\begin{cases} D_t^{\varepsilon} fal(e, \alpha, \delta) = \chi \\ D_t^{\varepsilon}\chi = -\dfrac{K_i}{K_d} fal(e, \alpha, \delta) - \dfrac{K_p}{K_d}\chi \end{cases} \tag{40}$$

Equation (40) can be rewritten as a matrix equation:

$$\begin{bmatrix} D_t^{\varepsilon} fal(e, \alpha, \delta) \\ D_t^{\varepsilon}(\chi) \end{bmatrix} = \begin{bmatrix} 0 & 1 \\ -\dfrac{K_i}{K_d} & -\dfrac{K_p}{K_d} \end{bmatrix} \begin{bmatrix} fal(e, \alpha, \delta) \\ \chi \end{bmatrix} \tag{41}$$

where $K_d > 0$, $K_i > 0$ and $K_p > 0$.

According to (6), (7), we know that the Fractional-order system (41) is stable if the following condition (42) is satisfied.

$$\begin{cases} |\arg(spec(\mathrm{Z}))| > \varepsilon\dfrac{\pi}{2} \\ 0 < \varepsilon\dfrac{\pi}{2} < \dfrac{1}{2}\pi \end{cases} \tag{42}$$

$$\dot{V} = \begin{cases} s\left(\begin{array}{l} K_p\alpha\,|e|^{\alpha-1}\left(\dot{\omega}_r + \frac{B}{J}\omega - \frac{3p_n\varphi_f}{2J}i_q + \frac{T_L}{J}\right) \\ + K_i D_t^{1-u} fal(e, \alpha, \delta) + K_d D_t^{\varepsilon+1} fal(e, \alpha, \delta) \end{array}\right) & if\ |e| > \delta \\ s\left(\begin{array}{l} K_p(1/\delta^{1-\alpha})\left(\dot{\omega}_r + \frac{B}{J}\omega - \frac{3p_n\varphi_f}{2J}i_q + \frac{T_L}{J}\right) \\ + K_i D_t^{1-u} fal(e, \alpha, \delta) + K_d D_t^{\varepsilon+1} fal(e, \alpha, \delta) \end{array}\right) & if\ |e| \le \delta \end{cases} \tag{34}$$

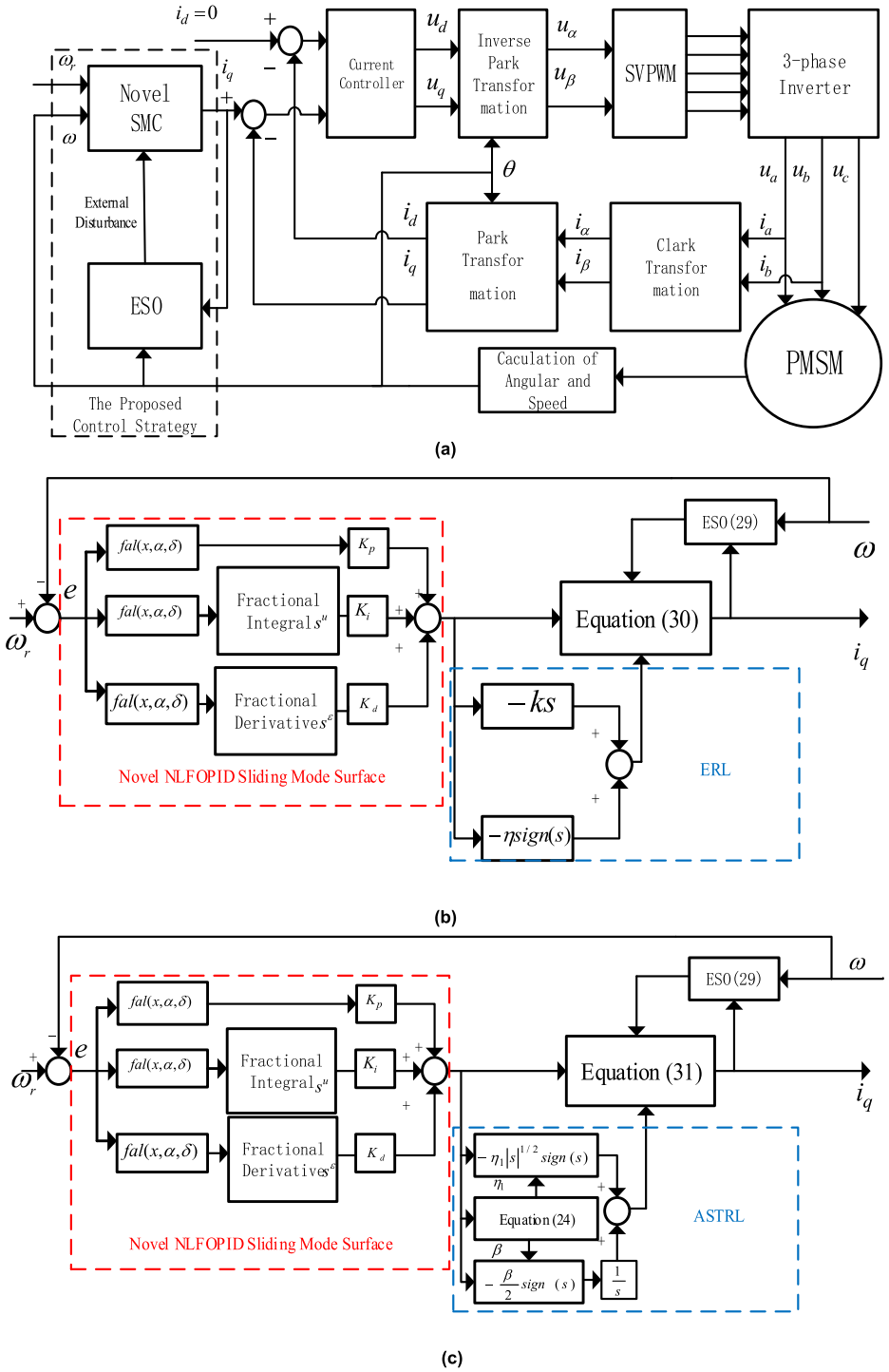

FIGURE 4. (a) The configuration of field-oriented control PMSM servo drive system based on the novel control strategy. (b) The proposed NLFOPIDSMC strategy. (c) The proposed ASTNLFOPIDSMC strategy.

where $Z = \begin{bmatrix} 0 & 1 \\ -\frac{K_i}{K_d} & -\frac{K_p}{K_d} \end{bmatrix}$, we know that the eigenvalues of matrix Z and $0 < \varepsilon < 1$ are synchronously satisfied the condition (42), then $|\arg(spec(Z))| > \varepsilon\frac{\pi}{2}$ holds, the system (41) is stable, consequently, the system (38) is also stable and its error decay towards 0 like $t^{-\varepsilon}$.

The stable domain in stable plane is shown in Fig. 5. To this end, the stable condition has been achieved.

The stability of the proposed ASTNLFOPIDSMC is discussed in the following theorem.

Proof: Step 1: when the amount of disturbances of the system is considered, then the following equation can be

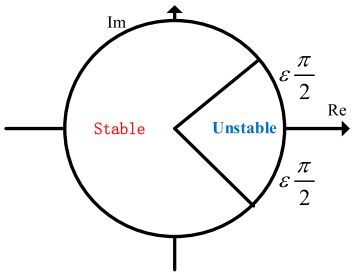

FIGURE 5. Stable domain of fractional order system.

derived:

$$\begin{cases} \dot{s} = -\eta_1 |s|^{1/2} sign(s) + \eta_2 + \Lambda \\ \begin{cases} \Lambda = K_p \alpha |e|^{\alpha-1} \Delta d & if \ |e| > \delta \\ \Lambda = K_p (1/\delta^{1-\alpha}) \Delta d & if \ |e| \le \delta \end{cases} \end{cases} \tag{43}$$

Assumption 2: The value of Λ has an upper limit, which satisfies the following condition:

$$|\Lambda| \le \hat{\delta} |s|^{1/2} \tag{44}$$

where $\hat{\delta} > 0$.

Then a new state variable is introduced:

$$\varphi = [\varphi_1, \varphi_2]^T = \left[|s|^{1/2} sign(s), \eta_2 \right]^T \tag{45}$$

According to (23), the time-derivative of φ could be expressed by the following:

$$\begin{cases} \dot{\varphi}_1 = \dfrac{1}{2|\varphi_1|} (-\eta_1 \varphi_1 + \varphi_2 + \Lambda) \\ \dot{\varphi}_2 = -\dfrac{\beta}{2|\varphi_1|} \varphi_1 \end{cases} \tag{46}$$

According to Assumption 2, Λ has the following form:

$$\Lambda = \phi(x,t) |s|^{1/2} sign(s) = \phi(x,t) \varphi_1 \tag{47}$$

where $0 < \phi(x,t) < \hat{\delta}$.

According to (46) and (47), it can be obtained as follows:

$$\begin{cases} \dot{\varphi} = \zeta \varphi \\ \zeta = \dfrac{1}{2|\varphi_1|} \begin{bmatrix} \phi(x,t) - \eta_1 & 1 \\ -\beta & 0 \end{bmatrix} \end{cases} \tag{48}$$

The positive definite Lyapunov function can be constructed as:

$$V = V_0 + \frac{1}{2\kappa_1} (\eta_1 - \tilde{\eta}_1)^2 + \frac{1}{2\kappa_2} (\beta - \tilde{\beta})^2 \tag{49}$$

where $\tilde{\eta}_1 > \eta_1, > 0, \tilde{\beta} > \beta > 0$ and $V_0 = \varphi^T P \varphi$, P is defined as follows:

$$P = \begin{bmatrix} \lambda + 4\theta^2 & -2\theta \\ -2\theta & 1 \end{bmatrix} \tag{50}$$

where λ is an arbitrary positive coefficient; the matrix P is positive definite symmetry, thus it is proved that the function V_0 is positive.

The first derivative of V_0 can be obtained as follows:

$$\begin{aligned} \dot{V}_0 &= \dot{\varphi}^T P \varphi + \varphi^T P \dot{\varphi} \\ &= \varphi^T (\zeta^T P + P \zeta) \varphi \\ &= -\frac{1}{2|\varphi_1|} \varphi^T \Theta \varphi \end{aligned} \tag{51}$$

where Θ is defined as follows:

$$\Theta = \begin{bmatrix} -2(\lambda + 4\theta^2)(\phi - \eta_1) - 4\theta\beta & 2\theta(\phi - \eta_1) + \beta - \lambda - 4\theta^2 \\ 2\theta(\phi - \eta_1) + \beta - \lambda - 4\theta^2 & 4\theta \end{bmatrix} \tag{52}$$

According to (24), we know $\beta = 2\theta\eta_1$, the matrix Θ will be positive definite with the minimum eigenvalue $\lambda_{\min}(\Theta) \ge 2\varepsilon$ if the follow condition (53) is satisfied.

$$\eta_1 > \frac{\hat{\delta}(\lambda + 4\theta^2)}{\lambda} + \frac{(2\varepsilon\hat{\delta} - \lambda - 4\theta^2)^2}{8\theta\lambda} \tag{53}$$

Sequentially, the derivation of (51) can be obtained as:

$$\dot{V}_0 \le -\frac{\theta}{|\varphi_1|} \varphi^T \varphi = -\frac{\theta}{|\varphi_1|} \|\varphi\|^2 \tag{54}$$

For the matrix Θ with maximum eigenvalue $\lambda_{\max}(\Theta)$, it is bounded by:

$$\lambda_{\min}(P) \|\varphi\|^2 \le \varphi^T P \varphi \le \lambda_{\max}(P) \|\varphi\|^2 \tag{55}$$

Then, Equation (45) can be rewritten as:

$$\|\varphi\|^2 = \varphi_1^2 + \varphi_2^2 = |s| + \varphi_2^2 \tag{56}$$

and

$$|s|^{1/2} \le \|\varphi\| \le \frac{V_0^{1/2}}{\lambda_{\min}^{1/2}(P)} \tag{57}$$

where $\lambda_{\max}(P)$, $\lambda_{\min}(P)$ are the maximum eigenvalue of matrix P and the minimum eigenvalue of matrix P, respectively.

Therefore, we can get:

$$\dot{V}_0 \le -\frac{\theta \lambda_{\min}^{1/2}(P)}{\lambda_{\max}(P)} V_0^{1/2} \tag{58}$$

The first derivative of V can be obtained as follows:

$$\begin{aligned} \dot{V} = \dot{V}_0 &+ \frac{1}{\kappa_1}(\eta_1 - \tilde{\eta}_1)\dot{\eta}_1 + \frac{1}{\kappa_2}(\beta - \tilde{\beta})\dot{\beta} \le -\frac{\theta \lambda_{\min}^{1/2}(P)}{\lambda_{\max}(P)} V_0^{1/2} \\ &- \frac{\gamma_1}{\sqrt{2\kappa_1}} |\eta_1 - \tilde{\eta}_1| - \frac{\gamma_2}{\sqrt{2\kappa_2}} \left| \beta - \tilde{\beta} \right| + \frac{1}{\kappa_1}(\eta_1 - \tilde{\eta}_1)\dot{\eta}_1 \\ &+ \frac{1}{\kappa_2}(\beta - \tilde{\beta})\dot{\beta} + \frac{\gamma_1}{\sqrt{2\kappa_1}} |\eta_1 - \tilde{\eta}_1| + \frac{\gamma_2}{\sqrt{2\kappa_2}} \left| \beta - \tilde{\beta} \right| \end{aligned} \tag{59}$$

According to the familiar inequality $\sqrt{x^2 + y^2 + z^2} \le |x| + |y| + |z|$, we can get:

$$\begin{aligned} \dot{V} \le -\tau \sqrt{V_0 + \frac{1}{2\kappa_1}(\eta_1 - \tilde{\eta}_1)^2 + \frac{1}{2\kappa_2}(\beta - \tilde{\beta})^2} \\ + \frac{1}{\kappa_1}(\eta_1 - \tilde{\eta}_1)\dot{\eta}_1 \\ + \frac{1}{\kappa_2}(\beta - \tilde{\beta})\dot{\beta} + \frac{\gamma_1}{\sqrt{2\kappa_1}} |\eta_1 - \tilde{\eta}_1| + \frac{\gamma_2}{\sqrt{2\kappa_2}} \left| \beta - \tilde{\beta} \right| \end{aligned} \tag{60}$$

where $\tau = \min \left\{ \frac{\theta \lambda_{\min}^{1/2}(P)}{\lambda_{\max}(P)}, \gamma_1, \gamma_2 \right\}$.

According to (47), we know $\eta_1 - \tilde{\eta}_1 < 0$ and $\beta - \tilde{\beta} < 0$, let

$$\begin{cases} \hat{V} = V_0 + \dfrac{1}{2\kappa_1}(\eta_1 - \tilde{\eta}_1)^2 + \dfrac{1}{2\kappa_2}(\beta - \tilde{\beta})^2 \\ \mathrm{X} = -|\eta_1 - \tilde{\eta}_1| \left(\dfrac{\dot{\eta}_1}{\kappa_1} - \dfrac{\gamma_1}{\sqrt{2\kappa_1}}\right) \\ \quad -\left|\beta - \tilde{\beta}\right| \left(\dfrac{\dot{\beta}}{\kappa_2} - \dfrac{\gamma_2}{\sqrt{2\kappa_2}}\right) \end{cases} \tag{61}$$

Then, (60) can be simplified to:

$$\dot{V} \leq -\tau \hat{V}^{1/2} + \mathrm{X} \tag{62}$$

Case I: $|s| > \nu$ and $\eta_1 > \hat{\eta}_1$.

$$\dot{\eta}_1 = \gamma_1 \sqrt{\frac{\kappa_1}{2}} \tag{63}$$

then

$$\mathrm{X} = -\left|\beta - \tilde{\beta}\right| \left(\frac{\dot{\beta}}{\kappa_2} - \frac{\gamma_2}{\sqrt{2\kappa_2}}\right) \tag{64}$$

Sequentially, let $\theta = \frac{\gamma_2}{2\gamma_1}\sqrt{\frac{\kappa_2}{\kappa_1}}$, it can be obtained as:

$$\dot{V} \leq -\tau V^{1/2} < 0 \tag{65}$$

Case II: $|s| > \nu$ and $\eta_1 \leq \hat{\eta}_1$.

$$\dot{\eta} = \Re \tag{66}$$

According to (24), we know the condition holds only for a short period of time, the value of η_1 will increase rapidly and satisfy condition $\eta_1 > \hat{\eta}_1$.

Case III: $|s| \leq \nu$ and $\eta_1 > \hat{\eta}_1$.

$$\dot{\eta}_1 = -\gamma_1 \sqrt{\frac{\kappa_1}{2}} \tag{67}$$

then

$$\mathrm{X} = 2\,|\eta_1 - \tilde{\eta}_1|\,\frac{\gamma_1}{\sqrt{2\kappa_1}} + \left|\beta - \tilde{\beta}\right| \left(\frac{2\varepsilon\gamma_1}{\kappa_2}\sqrt{\frac{\kappa_1}{2}} + \frac{\gamma_2}{\sqrt{2\kappa_2}}\right) \tag{68}$$

According to (67) (68), we know that $\mathrm{X} > 0$ and $\dot{\eta}_1 < 0$. Because of $\dot{\eta}_1 < 0$, $|s|$ will continue to increase until $|s| > \nu$. If the condition $|s| > \nu$ is satisfied, the $|s|$ will converge to 0, which means that s will be satisfied $|s| \leq \nu$ again. Therefore, it can be deduced that the sliding variable will remain in a domain $|s| \leq \nu_0$, and $\nu_0 > \nu$ in the sliding manifold.

Case IV: $|s| \leq \nu$ and $\eta_1 \leq \hat{\eta}_1$.

It has the similar procedure from the Case II with the $|s| > \nu$ and $\eta_1 \leq \hat{\eta}_1$.

In summary, it has proven that with the proposed ASTNLFOPIDSMC law, the system can reach the sliding surface at any initial state.

Step 2: We use the similar procedure from the step 2 of the proof of the NLFOPIDSMC.

Finally, the stable condition has been achieved.

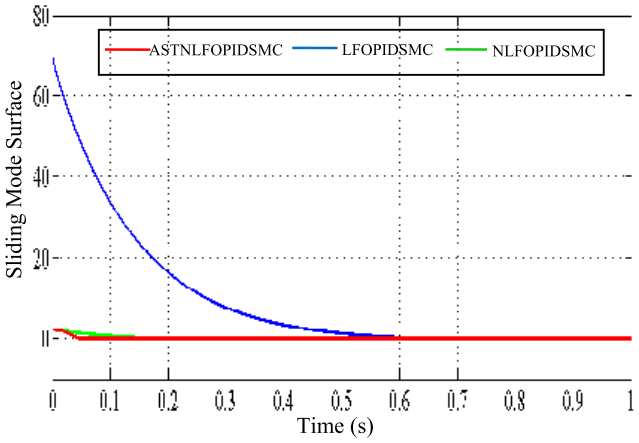

FIGURE 6. Response curves of the sliding mode functions under the traditional LFOPIDSMC, the proposed NLFOPIDSMC and the proposed ASTNLFOPIDSMC.

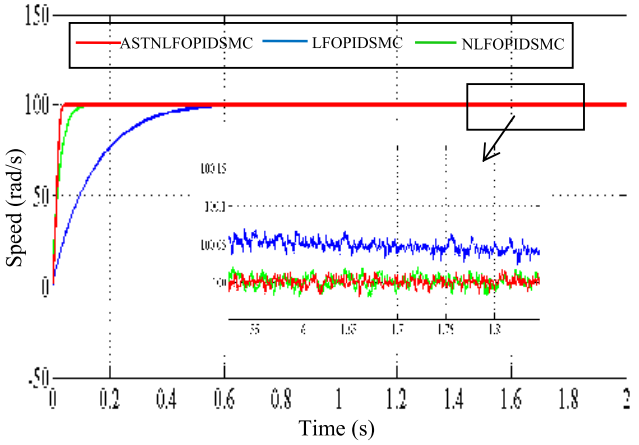

FIGURE 7. Speed response curves without load under three control strategies.

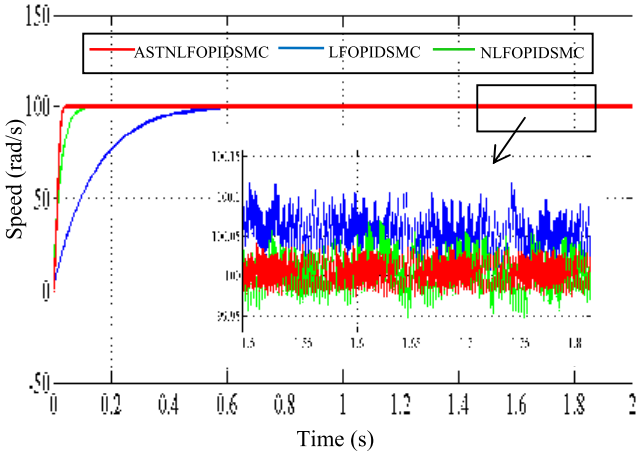

FIGURE 8. Speed response curves with $3N \cdot m$ load under three control strategies.

IV. COMPARATIVE SIMULATIONS

We simulate and validate the effectiveness and performance of the proposed approach used the PMSM verification platform based on Matlab/Simulink (R2014a).

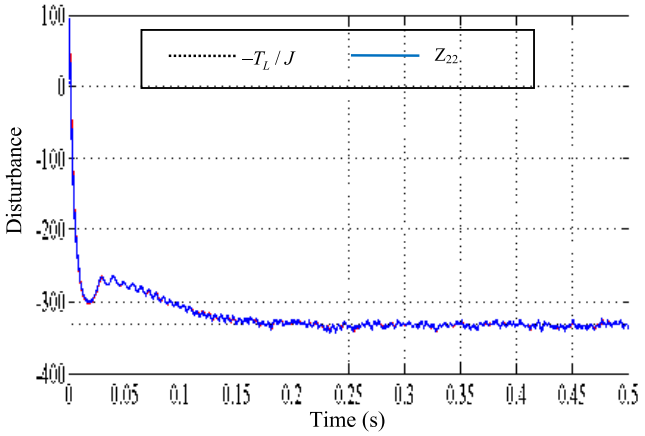

FIGURE 9. Tracking curves of disturbance under $3N \cdot m$ load based on the ESO.

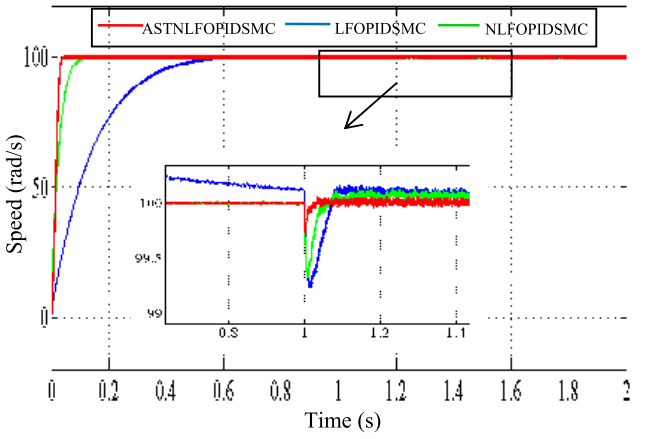

FIGURE 10. Speed response curves when the load suddenly increases.

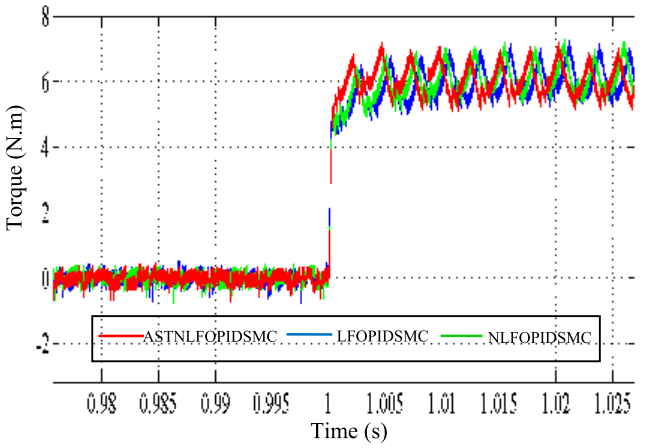

FIGURE 11. Electromagnetic torque response curves when the load suddenly increases.

The parameters of PMSM are listed as follows: $R_s = 0.958\Omega$, L = 5.25mH, $\varphi_f = 0.1827Wb$, J = $0.009kg \cdot m^2$, B = $0.008\ (Nm \cdot s)\ /rad$, $p_n = 4$. The key parameters of the conventional LFOPIDSMC are listed as follows: $K_p = 0.1$, $K_i = 0.3$, $K_d = 0.3$, $\varepsilon = 0.01$, $u = 0.01$, $k = 7$ and $\eta = 6$. The key parameters of the NLFOPIDSMC are listed as follows: $K_p = 0.1$, $K_i = 0.3$, $K_d = 0.3$, $\varepsilon = 0.01$, $u = 0.01$, $\delta = 0.1$, $\alpha = 0.25$, $k = 7$ and $\eta = 6$. The key parameters of the ASTNLFOPIDSMC are listed as follows: $K_p = 0.1$, $K_i = 0.3$, $K_d = 0.3$, $\varepsilon = 0.01$, $u = 0.01$, $\delta = 0.1$, $\alpha = 0.25$, $\nu = 0.05$, $\theta = 15$, $\gamma_1 = 10$, $\kappa_1 = 25$, $\hat{\eta}_1 = 0.01$, $\Re = 0.01$. Parameters of current loop PI controller are listed as follows: $\tilde{K}_p = 1100L$, $\tilde{K}_i = 1100R_s$. The parameters of the conventional ESO and novel ESO are listed as follows: $\omega_0 = 100$, $\tilde{\beta}_{01} = 200$, $\tilde{\beta}_{02} = 10000$, $\tilde{b}_0 = 121$, $\delta = 0.1$, $\alpha = 0.25$. The simulation results are shown in Figs. 6-13 and Tabs. 1-4.

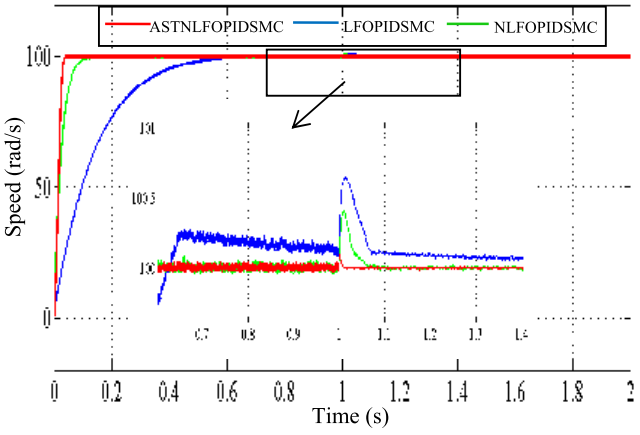

FIGURE 12. Speed response curves when the load suddenly decrease.

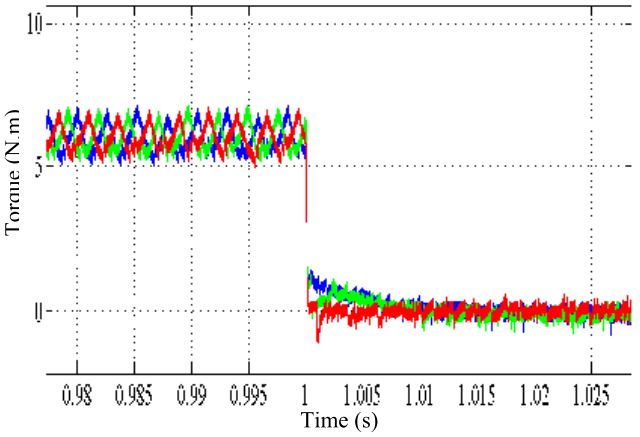

FIGURE 13. Electromagnetic torque response curves when the load suddenly decrease.

TABLE 1. Comparative results without load start-up.

Control Strategy	Reference Speed	Adjustment Time
LFOPIDSMC	100 rad/s	0.56 s
NLFOPIDSMC	100 rad/s	0.08 s
ASTNLFOPIDSMC	100 rad/s	0.04 s

Case I: sliding mode surface response comparison.

For the sake of simulation, a speed reference of 100 rad/s is given at 0 s, the response curves of the sliding mode

TABLE 2. Comparative results with load start-up.

Control Strategy	Reference Speed	Adjustment Time
LFOPIDSMC	100 rad/s	0.58 s
NLFOPIDSMC	100 rad/s	0.11 s
ASTNLFOPIDSMC	100 rad/s	0.05 s

TABLE 3. Comparative results of three control methods for sudden change of load from 0 $N \cdot m$ to 6 $N \cdot m$.

Control Strategy	Speed Recovery Time	Speed Overshoot Amount	Torque Setting Time
LFOPIDSMC	0.073 s	0.79%	0.0035 s
NLFOPIDSMC	0.053 s	0.67%	0.0031 s
ASTNLFOPIDSMC	0.032 s	0.23%	0.0022 s

TABLE 4. Comparative results of three control methods for sudden change of load from 6 $N \cdot m$ to 0 $N \cdot m$.

Control Strategy	Speed Recovery Time	Speed Overshoot Amount	Torque Setting Time
LFOPIDSMC	0.065 s	0.56%	0.0074 s
NLFOPIDSMC	0.057 s	0.42%	0.0065 s
ASTNLFOPIDSMC	0.015 s	0.12%	0.0024 s

surfaces under the proposed ASTNLFOPIDSMC, the proposed NLFOPIDSMC and the conventional LFOPIDSMC strategies are shown in Fig. 6.

Fig. 6 clearly demonstrates the time response curve of the proposed NLFOPID sliding surface is closer to $s = 0$ than the time response curve of the traditional LFOPID sliding surface. Furthermore, it is clear that the time to arrive at $s = 0$ under the proposed ASTNLFOPIDSMC strategy is shorter than those of the NLFOPIDSMC strategy and the traditional LFOPIDSMC strategy.

Case II: step response comparison.

A speed reference of 100 rad/s is given for 2 seconds. Fig. 7 reveals the speed response curves of ω without external load. While Fig. 8 reveals the speed response curves of ω with $3N \cdot m$ external load, and Fig. 9 reveals the estimated disturbance of the ESO. Finally, Tab. 1 and Tab. 2 show the speed adjustment time without and with load of the motor under the three control strategies, respectively. The following information can be obtained from Figs. 7-9, and Tabs. 1-2.

1) Speed response: the comparison of the speed response time is: "LFOPIDSMC > NLFOPIDSMC > ASTNLFOPIDSMC". It obviously shows that the ASTNLFOPIDSMC strategy has better dynamic performance.

2) Tracking error: when the system enters steady state, the tracking error of traditional LFOPIDSMC control method is larger than those of two novel control methods based on the novel NLFOPID sliding mode surface.

3) Chattering phenomenon: the chattering phenomenon of the LFOPIDSMC and the NLFOPIDSMC strategies are significantly larger than that of the ASTNLFOPIDSMC strategy.

4) ESO can estimate external disturbance accurately and timely.

The simulation results obviously demonstrate that the proposed ASTNLFOPIDSMC strategy exhibits not only improves system static and dynamic performance but also reduces chattering phenomenon effectively.

Case III: robustness performance comparison.

The following simulation compares the anti-interference capability of the three strategies under the external disturbance. A speed reference of 100 rad/s is given at 0 s, the external load torque T_L changes from $0N \cdot m$ to $6N \cdot m$ and from $6N \cdot m$ to $0N \cdot m$ at 1s, respectively. From Figs. 10-13, the comparisons of control performance are given when the external load disturbance is applied on the motor under the three control strategies. It can be seen from Figs. 10-13 that the three methods have different levels of impact caused by the external load disturbances. As can be seen from Fig. 10 and Fig. 12, the speed disturbance rejection recovery time of the ASTNLFOPIDSMC is significantly shorter than those of the LFOPIDSMC and the NLFOPIDSMC, and the speed fluctuation of the ASTNLFOPIDSMC is also smaller than those of the LFOPIDSMC and the NLFOPIDSMC. Fig. 11 and Fig. 13 reveal the electromagnetic torque curve under the three control strategies. According to the comparison results, we can clearly see that the proposed ASTNLFOPIDSMC has faster adjusting time of electromagnetic torque than those of the other control strategies. In order to better compare the anti-disturbance ability of the three control strategies, speed recovery time, speed overshoot amount and torque setting time are shown in Tabs. 3-4. As shown in the Tabs. 3-4, the performance indicators of the control system when the load suddenly increases and decreases, respectively. Evidently, the comparison results confirm that the proposed ASTNLFOPIDSMC controller exhibits better robustness against external disturbances than other control methods.

In summary, the comparative results have clearly demonstrated that the proposed ASTFOPIDSMC strategy not only achieves better control performance with good stability and dynamic properties, but also it has very strong robustness.

V. CONCLUSION AND FUTURE WORK

A novel ESO based ASTNLFOPIDSMC strategy for the speed operation of PMSM is successfully proposed. First of all, we propose a novel NLFOPID sliding mode surface with nonlinear proportion term, nonlinear integral term and nonlinear differential term; secondly, a novel ASTNLFOPIDSMC strategy is constructed by the ASTRL and the novel NLFOPID sliding surface; and then, ESO is designed to estimate the value of the external disturbance; then, a novel compound control strategy based on the ESO and the ASTNLFOPIDSMC for the speed operation of PMSM is proposed; finally, comparison results show that the proposed control strategy not only achieves good stability and dynamic performance, but is also robust to external disturbance.

The application of the novel NLFOPID sliding surface and the ASTRL leads to an increase in the parameters of the proposed ASTNLFOPIDSMC strategy, thus increasing the complexity of the proposed ASTNLFOPIDSMC strategy. For future work, we will use an optimization algorithm to complete the selection of the parameters of the proposed ASTNLFOPIDSMC strategy, which will further improve the performance of the proposed ASTNLFOPIDSMC strategy.

REFERENCES

[1] B. Xu, X. Shen, W. Ji, G. Shi, J. Xu, and S. Ding, "Adaptive nonsingular terminal sliding model control for permanent magnet synchronous motor based on disturbance observer," *IEEE Access*, vol. 6, pp. 48913–48920, 2018.

[2] X. Zhang, L. Sun, K. Zhao, and L. Sun, "Nonlinear speed control for PMSM system using sliding-mode control and disturbance compensation techniques," *IEEE Trans. Power Electron.*, vol. 28, no. 3, pp. 1358–1365, Mar. 2013.

[3] B. Sneyers, D. W. Novotny, and T. A. Lipo, "Field weakening in buried permanent magnet AC motor drives," *IEEE Trans. Ind. Appl.*, vol. IA-21, no. 2, pp. 398–407, Mar. 1985.

[4] S. Li and Z. Liu, "Adaptive speed control for permanent-magnet synchronous motor system with variations of load inertia," *IEEE Trans. Ind. Electron.*, vol. 56, no. 8, pp. 3050–3059, Aug. 2009.

[5] Q. Wang, H. Yu, M. Wang, and X. Qi, "An improved sliding mode control using disturbance torque observer for permanent magnet synchronous motor," *IEEE Access*, vol. 7, pp. 36691–36701, 2019.

[6] S.-K. Kim, J.-S. Lee, and K.-B. Lee, "Offset-free robust adaptive backstepping speed control for uncertain permanent magnet synchronous motor," *IEEE Trans. Power Electron.*, vol. 31, no. 10, pp. 7065–7076, Oct. 2016.

[7] S.-F. Wu, J.-W. Zhang, and B.-B. Chai, "A robust backstepping sensorless control for interior permanent magnet synchronous motor using a super-twisting based torque observer," *Asian J. Control*, vol. 21, no. 1, pp. 172–183, Jan. 2019.

[8] S. Li, H. Liu, and S. Ding, "A speed control for a PMSM using finite-time feedback control and disturbance compensation," *Trans. Inst. Meas. Control*, vol. 32, no. 2, pp. 170–187, Apr. 2010.

[9] M. Preindl and S. Bolognani, "Model predictive direct speed control with finite control set of PMSM drive systems," *IEEE Trans. Power Electron.*, vol. 28, no. 2, pp. 1007–1015, Feb. 2013.

[10] H. Chaoui and P. Sicard, "Adaptive fuzzy logic control of permanent magnet synchronous machines with nonlinear friction," *IEEE Trans. Ind. Electron.*, vol. 59, no. 2, pp. 1123–1133, Feb. 2012.

[11] C.-K. Lai and K.-K. Shyu, "A novel motor drive design for incremental motion system via sliding-mode control method," *IEEE Trans. Ind. Electron.*, vol. 52, no. 2, pp. 499–507, Apr. 2005.

[12] S. Li, M. Zhou, and X. Yu, "Design and implementation of terminal sliding mode control method for PMSM speed regulation system," *IEEE Trans Ind. Informat.*, vol. 9, no. 4, pp. 1879–1891, Nov. 2013.

[13] M. A. M. Cheema, J. E. Fletcher, M. Farshadnia, and M. F. Rahman, "Sliding mode based combined speed and direct thrust force control of linear permanent magnet synchronous motors with first-order plus integral sliding condition," *IEEE Trans. Power Electron.*, vol. 34, no. 3, pp. 2526–2538, Mar. 2019.

[14] Y. Lee, S.-H. Lee, and C.-C. Chung, "LPV $\mathcal{H}_\infty$ control with disturbance estimation for permanent magnet synchronous motors," *IEEE Trans. Ind. Electron.*, vol. 65, no. 1, pp. 488–497, Jan. 2018.

[15] D. Yao, B. Zhang, P. Li, and H. Li, "Event-triggered sliding mode control of discrete-time Markov jump systems," *IEEE Trans. Syst., Man, Cybern., Syst.*, vol. 49, no. 10, pp. 2016–2025, Oct. 2019.

[16] Y. Deng, J. Wang, H. Li, J. Liu, and D. Tian, "Adaptive sliding mode current control with sliding mode disturbance observer for PMSM drives," *ISA Trans.*, vol. 88, pp. 113–126, May 2019.

[17] C. Jing, H. Xu, and X. Niu, "Adaptive sliding mode disturbance rejection control with prescribed performance for robotic manipulators," *ISA Trans.*, vol. 91, pp. 41–51, Aug. 2019.

[18] V. Q. Leu, H. H. Choi, and J.-W. Jung, "Fuzzy sliding mode speed controller for PM synchronous motors with a load torque observer," *IEEE Trans. Power Electron.*, vol. 27, no. 3, pp. 1530–1539, Mar. 2012.

[19] L. Sheng, W. Li, Y. Wang, M. Fan, and X. Yang, "Sensorless control of a shearer short-range cutting interior permanent magnet synchronous motor based on a new sliding mode observer," *IEEE Access*, vol. 5, pp. 18439–18450, 2017.

[20] K. Zhao, T. Yin, C. Zhang, J. He, X. Li, Y. Chen, R. Zhou, and A. Leng, "Robust model-free nonsingular terminal sliding mode control for PMSM demagnetization fault," *IEEE Access*, vol. 7, pp. 15737–15748, 2019.

[21] L. Yubo and W. Xudong, "Speed global integral sliding mode control with a load sliding mode observer for PMSM," *IEICE Electron. Exp.*, vol. 15, no. 6, 2018, Art. no. 20171270.

[22] J.-J. Xiong and G.-B. Zhang, "Global fast dynamic terminal sliding mode control for a quadrotor UAV," *ISA Trans.*, vol. 66, pp. 233–240, Jan. 2017.

[23] F.-J. Lin, P.-H. Chou, C.-S. Chen, and Y.-S. Lin, "DSP-based cross-coupled synchronous control for dual linear motors via intelligent complementary sliding mode control," *IEEE Trans. Ind. Electron.*, vol. 59, no. 2, pp. 1061–1073, Feb. 2012.

[24] J. Yan, H. Wang, S. Huang, and Y. Lan, "Load disturbance observer-based complementary sliding mode control for PMSM of the mine traction electric locomotive," *Int. J. Fuzzy Syst.*, vol. 21, no. 4, pp. 1051–1058, Jun. 2019.

[25] C. B. Kadu, A. A. Khandekar, and C. Y. Patil, "Design of sliding mode controller with proportional integral sliding surface for robust regulation and tracking of process control systems," *J. Dyn. Syst., Meas., Control*, vol. 140, no. 9, Sep. 2018, Art. no. 091004.

[26] A. J. Muñoz-Vázquez, F. Gaxiola, F. Martínez-Reyes, and A. Manzo-Martínez, "A fuzzy fractional-order control of robotic manipulators with PID error manifolds," *Appl. Soft Comput.*, vol. 83, Oct. 2019, Art. no. 105646.

[27] H. L. N. N. Thanh and S. K. Hong, "Quadcopter robust adaptive second order sliding mode control based on PID sliding surface," *IEEE Access*, vol. 6, pp. 66850–66860, 2018.

[28] S. Mobayen, "An adaptive chattering-free PID sliding mode control based on dynamic sliding manifolds for a class of uncertain nonlinear systems," *Nonlinear Dyn.*, vol. 82, nos. 1–2, pp. 53–60, Oct. 2015.

[29] Y. Wang, F. Yan, J. Chen, F. Ju, and B. Chen, "A new adaptive time-delay control scheme for cable-driven manipulators," *IEEE Trans Ind. Informat.*, vol. 15, no. 6, pp. 3469–3481, Jun. 2019.

[30] Y. Wang, F. Yan, K. Zhu, B. Chen, and H. Wu, "A new practical robust control of cable-driven manipulators using time-delay estimation," *Int. J. Robust Nonlinear Control*, vol. 29, no. 11, pp. 3405–3425, Jul. 2019.

[31] Y. Wang, L. Liu, D. Wang, F. Ju, and B. Chen, "Time-delay control using a novel nonlinear adaptive law for accurate trajectory tracking of cable-driven robots," *IEEE Trans Ind. Informat.*, to be published, doi: 10.1109/TII.2019.2951741.

[32] S. Song, B. Zhang, J. Xia, and Z. Zhang, "Adaptive backstepping hybrid fuzzy sliding mode control for uncertain fractional-order nonlinear systems based on finite-time scheme," *IEEE Trans. Syst., Man, Cybern. Syst.*, to be published, doi: 10.1109/TSMC.2018.2877042.

[33] S. Song, J. H. Park, B. Zhang, and X. Song, "Observer-based adaptive hybrid fuzzy resilient control for fractional-order nonlinear systems with time-varying delays and actuator failures," *IEEE Trans. Fuzzy Syst.*, to be published, doi: 10.1109/TFUZZ.2019.2955051.

[34] S. Song, B. Zhang, X. Song, and Z. Zhang, "Neuro-fuzzy-based adaptive dynamic surface control for fractional-order nonlinear strict-feedback systems with input constraint," *IEEE Trans. Syst., Man, Cybern., Syst.*, to be published, doi: 10.1109/TSMC.2019.2933359.
[35] B. Zhang, Y. Pi, and Y. Luo, "Fractional order sliding-mode control based on parameters auto-tuning for velocity control of permanent magnet synchronous motor," *ISA Trans.*, vol. 51, no. 5, pp. 649–656, Sep. 2012.
[36] X. Rui, W. Yin, Y. Dong, L. Lin, and X. Wu, "Fractional-order sliding mode control for hybrid drive wind power generation system with disturbances in the grid," *Wind Energy*, vol. 22, no. 1, pp. 49–64, Jan. 2019.
[37] K. K. Ayten, M. H. Çiplak, and A. Dumlu, "Implementation a fractional-order adaptive model-based PID-type sliding mode speed control for wheeled mobile robot," *Proc. Inst. Mech. Eng. I, J. Syst. Control Eng.*, vol. 233, no. 8, pp. 1067–1084, Sep. 2019.
[38] Q. Gao, Y.-L. Hou, J.-B. Liu, R.-M. Hou, M.-M. Lv, L. Wang, and C. Wang, "An extended state observer based fractional order sliding-mode control for a novel electro-hydraulic servo system with iso-actuation balancing and positioning," *Asian J. Control*, vol. 21, no. 1, pp. 289–301, Jan. 2019.
[39] F. M. Zaihidee, S. Mekhilef, and M. Mubin, "Application of fractional order sliding mode control for speed control of permanent magnet synchronous motor," *IEEE Access*, vol. 7, pp. 101765–101774, 2019.
[40] J. Song, L. Wang, G. Cai, and X. Qi, "Nonlinear fractional order proportion-integral-derivative active disturbance rejection control method design for hypersonic vehicle attitude control," *Acta Astronautica*, vol. 111, pp. 160–169, Jun./Jul. 2015.
[41] L. Shi, X. Miao, and H. Wang, "An improved nonlinear proportional-integral-differential controller combined with fractional operator and symbolic adaptation algorithm," *Trans. Inst. Meas. Control*, Oct. 2019, Art. no. 014233121987933.
[42] J. Han, "From PID to active disturbance rejection control," *IEEE Trans. Ind. Electron.*, vol. 56, no. 3, pp. 900–906, Mar. 2009.
[43] Q. Li, J. Yuan, and B. Zhang, "Extended state observer based output control for spacecraft rendezvous and docking with actuator saturation," *ISA Trans.*, vol. 88, pp. 37–49, May 2019.
[44] C. Hua, J. Li, Y. Yang, and X. Guan, "Extended-state-observer-based finite-time synchronization control design of teleoperation with experimental validation," *Nonlinear Dyn.*, vol. 85, no. 1, pp. 317–331, Jul. 2016.
[45] W. Xu, R. Dian, Y. Liu, D. Hu, and J. Zhu, "Robust flux estimation method for linear induction motors based on improved extended state observers," *IEEE Trans. Power Electron.*, vol. 34, no. 5, pp. 4628–4640, May 2019.
[46] Y. Wang, J. Chen, F. Yan, K. Zhu, and B. Chen, "Adaptive super-twisting fractional-order nonsingular terminal sliding mode control of cable-driven manipulators," *ISA Trans.*, vol. 86, pp. 163–180, Mar. 2019.
[47] Y. Shtessel, M. Taleb, and F. Plestan, "A novel adaptive-gain supertwisting sliding mode controller: Methodology and application," *Automatica*, vol. 48, no. 5, pp. 759–769, May 2012.
[48] A.-R. Babaei, M. Malekzadeh, and D. Madhkhan, "Adaptive super-twisting sliding mode control of 6-DOF nonlinear and uncertain air vehicle," *Aerosp. Sci. Technol.*, vol. 84, pp. 361–374, Jan. 2019.
[49] S.-D. Lee, B. D. Hong Phuc, X. Xu, and S.-S. You, "Roll suppression of marine vessels using adaptive super-twisting sliding mode control synthesis," *Ocean Eng.*, vol. 195, Jan. 2020, Art. no. 106724.
[50] Z. Sun, J. Zheng, Z. Man, M. Fu, and R. Lu, "Nested adaptive super-twisting sliding mode control design for a vehicle steer-by-wire system," *Mech. Syst. Signal Process.*, vol. 122, pp. 658–672, May 2019.
[51] Y. Wang, K. Zhu, F. Yan, and B. Chen, "Adaptive super-twisting nonsingular fast terminal sliding mode control for cable-driven manipulators using time-delay estimation," *Adv. Eng. Softw.*, vol. 128, pp. 113–124, Feb. 2019.
[52] S. Mobayen, F. Tchier, and L. Ragoub, "Design of an adaptive tracker for n-link rigid robotic manipulators based on super-twisting global nonlinear sliding mode control," *Int. J. Syst. Sci.*, vol. 48, no. 9, pp. 1990–2002, Jul. 2017.
[53] T. Li, A. M. Esteban, and S. Zhang, "Enhanced disturbance rejection control based test rocket control system design and validation," *ISA Trans.*, vol. 84, pp. 31–42, Jan. 2019.
[54] I. Podlubny, "Fractional-order systems and PI^{λ}-D^{μ}-controllers," *IEEE Trans. Automat. Control*, vol. 44, no. 1, pp. 208–214, Jan. 1999.
[55] A.-A. Kilbas, H.-M. Srivastava, and J.-J. Trujillo, *Theory and Applications of Fractional Differential Equations* (North-Holland Mathematics Studies). Amsterdam, The Netherlands: North Holland, 2006.
[56] E. Ahmed, A. M. A. El-Sayed, and H. A. A. El-Saka, "Equilibrium points, stability and numerical solutions of fractional-order predator–prey and rabies models," *J. Math. Anal. Appl.*, vol. 325, no. 1, pp. 542–553, Jan. 2007.

PENG GAO received the B.S. degree in electronic information engineering and the M.S. degree in power electronics and electric drive from the Anhui University of Technology, Maanshan, China, in 2007 and 2010, respectively. He is currently pursuing the Ph.D. degree in power engineering automation with Nanjing Tech University, Nanjing, China. His research interests include advanced control theory and its application to mechatronics.

GUANGMING ZHANG received the B.Eng. degree from Nanjing Tech University, Nanjing, China, in 1988, and the M.Eng. and Ph.D. degrees from the PLA University of Science and Technology, in 1998 and 2002, respectively.

Since 1998, he has been with the College of Electrical Engineering and Control Science, Nanjing Tech University, where he is currently a Professor. He has published more than 80 articles in journals and international conferences. His major research interest includes advanced control theory for mechatronics.

HUIMIN OUYANG (Member, IEEE) received the B.Eng. degree from the Tianjin Institute of Urban Construction, Tianjin, China, in 2005, the M.Eng. degree from the Nagoya Institute of Technology, Nagoya, Japan, in 2009, and the Ph.D. degree from the Toyohashi University of Technology, Toyohashi, Japan, in 2012. Since 2013, he has been with the College of Electrical Engineering and Control Science, Nanjing Tech University, Nanjing, China, where he is currently an Assistant Professor. He has published more than 30 articles in journals and international conferences. His major research interests include system control theory and its application to mechatronics.

LEI MEI (Member, IEEE) received the B.Eng. degree from the Jiangsu University of Science and Technology, Zhenjiang, China, in 2000, and the Ph.D. degree from the Nanjing University of Aeronautics and Astronautics, in 2009. Since 2009, he has been with the College of Electrical Engineering and Control Science, Nanjing Tech University, Nanjing, China, where he is currently an Associate Professor. He has published more than 20 articles in journals and international conferences. His major research interests include motor design and flywheel energy storage technology and application.